Atomic-electron capture in the presence of a narrow nuclear resonance: $^{40}Ar(p,p)^{40}Ar$ reaction

A. D. González,* J. P. Giese,† and E. Horsdal-Pedersen
Institute of Physics and Astronomy, Aarhus University, DK-8000 Aarhus C, Denmark
(Received 11 November 1992)

Electron capture in close, energetic collisions between protons and Ar atoms is studied. As the proton energy is varied across the 1859.7-keV $^{40}Ar(p,p)^{40}Ar$ elastic nuclear resonance at a fixed deflection angle of 60°, a dip of about 27% in the atomic-electron-capture probability is found, demonstrating the influence of the nuclear process on the atomic-charge exchange. The effect is very large considering that the similar dip found in the probability for scattering the proton without capture is only about 37%. A systematic comparison with previously reported capture probabilities for other elastic reactions has been made.

PACS number(s): 34.70.+e, 24.30.−v, 34.50.Fa

I. INTRODUCTION

A close collision between an atom and an energetic proton may lead to a strong deflection of the proton and ionization of the atom. The ionization is described exclusively by atomic parameters if the proton is scattered elastically by the pure Coulomb part of the internuclear force, but in case a transient compound nucleus is formed during the collision, the ionization depends also on the parameters describing the compound nuclear state. In recent years, there have been a number of studies on this interplay between atomic and nuclear processes. Most of them have concentrated on the influence of nuclear reactions on the ionization to continuum states of target inner-shell electrons, but there are also a few studies of ionization by charge transfer near elastic nuclear resonances [1–4].

The theoretical study of electron capture at large deflection angles and near nuclear resonances has resulted in two theoretical approaches: One based on the strong-potential Born approximation (SPB) [5,6] or its on-shell version, the impulse approximation (IA) [7], and the other on a generalization of the two-amplitude Blair-Anholt formula developed for ionization [8]. In the SPB approach, the capture amplitude near a nuclear reaction may be expressed as a sum of three terms which describe capture due to the Coulomb interaction between projectile and electron outside (the Coulomb term) or inside (the nuclear-volume term) a small spherical volume around the nucleus, and capture due to target recoil (the recoil term) [9]. The Coulomb term describes the three time sequences *enc*, *nec*, and *ecn*, where *e* symbolizes excitation of the electron, *c* electron capture, and *n* nuclear scattering. The sequences *enc* and *nec* thus describe excitation before and after the nuclear scattering, respectively, followed by attachment of the electron to the projectile, while *ecn* describes excitation and capture prior to the nuclear scattering. The Coulomb term and its three sequences are also present in the absence of nuclear resonances. The recoil term is always present for large deflection angles. However, the nuclear-volume term is present only for rapidly varying nuclear-scattering amplitudes, i.e., at nuclear resonances. It has two contributions corresponding to the sequence *enc* and *nec*.

The two-amplitude formulation contains a Coulomb, a nuclear-volume, and a recoil term like the SPB or IA. These terms can be combined into two terms which represent the sequences *ecn* and *nec*, but the contribution from the sequence *enc* is neglected. The formulation involves electronic amplitudes to be calculated for a prescribed broken straight-line nuclear trajectory [10]. Both theoretical treatments have shown general agreement when compared to experimental results.

The interplay between nuclear and atomic processes in atomic-charge transfer is seen as an anomaly in the energy dependence of the probability for the atomic process at the nuclear resonance. This anomaly is due to a rapidly changing interference between inelastic half-trajectory amplitudes separated by the nuclear reaction. A simple criterion for a strong atomic-nuclear interplay in electron capture is [5,6]

$$\frac{\Delta E}{\Gamma}=\frac{\varepsilon_f-\varepsilon_i+mv^2/2}{\Gamma}\geq 1\ , \tag{1}$$

where $\varepsilon_{i,f}$ (negative numbers) are the initial and final energies of the captured electron relative to the target and projectile, respectively, v is the projectile velocity in the laboratory frame, Γ the width of the nuclear resonance, and m is the electron mass. The final-state energy of the electron relative to the ionization limit of the target atom, $\varepsilon_f+mv^2/2$, is well defined for capture but not for pure ionization reactions in which the kinetic energy $\frac{1}{2}mv^2$ of the ejected electron is normally unknown. The term $\frac{1}{2}mv^2$ contributes to making the energy transfer ΔE relatively large for capture and comparable to the width of the nuclear resonance in a number of reactions.

The general criterion expressed through Eq. (1) for a strong influence of the nuclear resonance may be understood as follows: If the atomic inelastic-energy transfer ΔE is larger than or of the order of the width Γ of the elastic nuclear resonance, and in addition the initial projectile energy $E\approx E_R+\Delta E$, where E_R is the resonance energy, then the energy transfer ΔE will shift the energy of the projectile to the nuclear resonance if it takes place

while the nuclei are still approaching. The terms *enc* and *ecn* will thus involve the nuclear-scattering resonance, whereas the term *nec* will be off resonance. At the lower energy $E \approx E_R$, the terms *enc* and *ecn* will now be off resonance, while the term *nec* will be on. If $\Delta E \gg \Gamma$, one therefore observes two separate resonance structures (at $E = E_R$ and $E = E_R + \Delta E$) of a certain strength. However, if $\Delta E \approx \Gamma$, all terms of the capture amplitude vary near the resonance, and therefore one interference structure at $E = E_R$ is expected. Finally, if $\Delta E \ll \Gamma$, all terms of the capture amplitude are simply proportional to some common nuclear-scattering amplitude, and no special atomic-interference structure due to nuclear effects is predicted. Nevertheless, the various atomic half-trajectory amplitudes still interfere. This may lead to a strong angular dependence of the capture amplitude both on and off resonance.

The magnitude of the excursion of the probability for electron capture from a given atomic shell due to an elastic nuclear reaction depends not only on the ratio $\Delta E/\Gamma$, but also on the strength of the scattering resonance relative to the smooth Coulomb background scattering. Therefore, in order to compare the influence of resonances with different values of $\Delta E/\Gamma$, a normalization to the resonance strength is required. When the available data [11–16] are normalized in this way, a fair agreement with the basic criterion (1) is found.

In the present work, we report on atomic-electron-capture probabilities across the elastic nuclear resonance ^{40}Ar$(p,p)^{40}$Ar at 1859.7 keV. The width Γ of this resonance is 1288 eV [17] and the ratio $\Delta E/\Gamma$ is equal to 1.0 for capture from the L shell [18] which gives the dominant contribution to the total cross section. A dip in the capture probability of close to 27% is observed near the nuclear resonance which is a very strong effect when compared to the proton-scattering resonance intensity which is only 37%. The strong influence is expected considering that $\Delta E/\Gamma$ is close to 1 in the present case. The size of the measured resonance structure in the capture probability is in good agreement with calculations based on the IA model, but the theoretical shape is somewhat different from the experimental one, and theory overestimates the data in absolute value by nearly a factor of 2. Off-resonance electron-capture probabilities as a function of the laboratory proton-scattering angle were also measured.

II. EXPERIMENTAL SETUP AND PROCEDURE

Figure 1 shows the experimental setup. The proton beam was obtained from the 6-MV Aarhus University tandem accelerator. After passing through a set of 2×2 mm^2 collimators, the proton beam traversed a cell with Ar gas and was finally collected in a Faraday cup after the interaction region.

A position-sensitive surface-barrier detector (PSSB) placed at 60° relative to the beam direction and covering a solid angle of 7×10^{-3} sr was used to detect scattered, neutralized particles (H^0). A strong permanent magnet gave a field of nearly 10 kG over a 5-cm-long part of the 12-cm beam path between the gas cell and the position-sensitive detector. The protons were deflected sufficiently by this field to clearly distinguish the neutralized particles from scattered protons. The permanent magnet could be removed for measuring the protons and neutral particles together on the detector. In addition, for normalization purposes, the particles scattered into a solid angle of 4×10^{-3} sr around a laboratory angle of 52.5° were counted by means of a surface-barrier (SB) detector. In order to scan the beam energy across the elastic nuclear resonance without changing the accelerator-voltage or beam-transport settings, a post-acceleration voltage in the range -0.5 to -4.5 kV was applied on the Ar-gas cell. Thin Al foils placed directly in front of each detector served to stop secondary electrons from the negatively charged target.

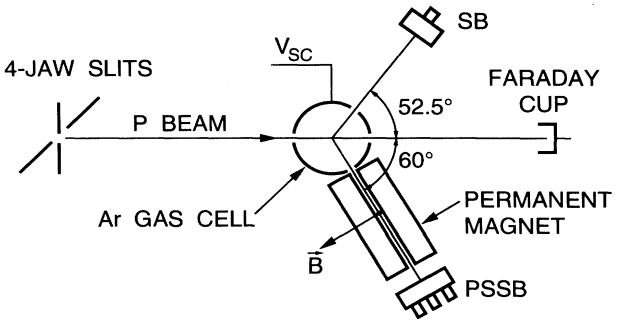

FIG. 1. Experimental setup. The position-sensitive surface-barrier detector (PSSB) is placed at 60°. A removable permanent magnet is used for separating the neutral H^0 and the scattered charged particles. The other surface-barrier (SB) detector at 52.5° is used for normalization. V_{sc} represents the voltage applied on the electrically floated target cell. It is the sum of a scanning voltage and the accelerator HV ripple multiplied by 2.

The Aarhus tandem accelerator can be run under computer control. In this way, the field in the analyzing magnet, which defines the energy of the beam from the accelerator, can be set at a constant value with fluctuations smaller than 1×10^{-5}. Long-term drift in the magnetic field, which would broaden the resonance, is thus avoided. The width of the 1859.7-keV ^{40}Ar$(p,p)^{40}$Ar resonance studied here is 1288 eV [17]. The accelerator-voltage ripple is of the order of 500 V FWHM (full width at half maximum). This leads to an energy spread of about 1 keV, which would cause a significant broadening of the resonance and blur its influence on the capture probability. Therefore, a technique for compensating the accelerator-voltage ripple was developed. Briefly, the target region is electrically isolated from ground and forced to follow two times the voltage fluctuations of the accelerator terminal by means of a fast HV power supply. The factor of 2 is due to the double acceleration of the protons in the tandem accelerator. A beam-energy spread as small as 95 eV on the target was achieved, which is 13 times smaller than the width of the resonance studied here. A detailed account of this technique has been published elsewhere [17].

The capture probability for a given scattering angle θ and energy E is defined by

$$p(E,\theta)=\frac{n^0(E,\theta)}{N_{\text{scatt}}(E,\theta)} , \tag{2}$$

where $n^0(E,\theta)$ is the number of neutral particles and $N_{\text{scatt}}(E,\theta)$ the total number of particles scattered into a given solid angle around the laboratory angle θ at the beam energy E.

Even at the relatively strong beam intensities up to 5 μA used in the present experiment, the counting rates were low, and thus the solid angles covered by the detectors had to be as large as possible. Therefore the beam paths from the target cell to the detectors were quite open. As a consequence, the beams on the PSSB detector were broad, and a strong magnetic field was required to separate them. The detector was placed such as to accommodate all neutral particles, but this had the disadvantage that some of the protons were deflected off the detector. It was therefore not possible to simultaneously measure $n^0(E,\theta)$ and $N_{\text{scatt}}(E,\theta)$. However, an independent measurement without the magnet gave the ratio between the counting rates of the two detectors; at $\theta_1=60°$ and $\theta_2=52.5°$ it reads

$$R(E,\theta_1,\theta_2)=\frac{N_{\text{scatt}}(E,\theta_1)}{N_{\text{scatt}}(E,\theta_2)} , \tag{3}$$

and then the capture probability given by Eq. (2) can be written as

$$p(E,\theta_1)=\frac{n^0(E,\theta_1)}{R(E,\theta_1,\theta_2)N_{\text{scatt}}(E,\theta_2)} , \tag{4}$$

where $n^0(E,\theta_1=60°)$ and $N_{\text{scatt}}(E,\theta_2=52.5°)$ are measured simultaneously in a run with the permanent magnet in place.

Figures 2(a) and 2(b) show the 1859.7-keV ^{40}Ar$(p,p)^{40}$Ar elastic resonance as seen by the detectors at 52.5° and 60°, respectively, and without magnetic deflection. Using a least-squares fitting routine and Poisson statistics, the resonance shapes in Figs. 2(a) and 2(b) were fitted by the appropriate expression [19] for a single, narrow resonance,

$$\frac{d\sigma}{d\Omega}=\frac{\frac{1}{4}A\Gamma^2+\frac{1}{2}B\Gamma(E_0-E)}{(E_0-E)^2+\frac{1}{4}\Gamma^2}+C . \tag{5}$$

The angular-dependent parameters A and B give the shape and size of the resonance, and C is a constant background from Coulomb scattering.

The energy-dependent ratio R [Eq. (3)] was then obtained from the fitted curves and is plotted in Fig. 3. The observed increase and decrease of the ratio R are due to the difference in shape of the resonance observed in the directions 52.5° and 60°.

To measure the capture probability near the resonance, we have proceeded as follows. First, the resonance was found by counting scattered particles without magnetic deflection while scanning the target acceleration voltage (V_{sc} in Fig. 1) over a range of 4 kV (see Fig. 2) for different fixed accelerator voltages near the expected value of the known resonance energy. Then the permanent magnet was mounted, and for a selected accelerator voltage, the scanning voltage V_{sc} was used to repeatedly cycle through five different beam energies separated by 1 keV. At each energy, scattered particles were detected by the PSSB at 60° and the SB at 52.5° and accumulated for a period of 1 min and then added to a position spectrum and a scaler, respectively, belonging to that energy. At the end of each cycle of five energies, a con-

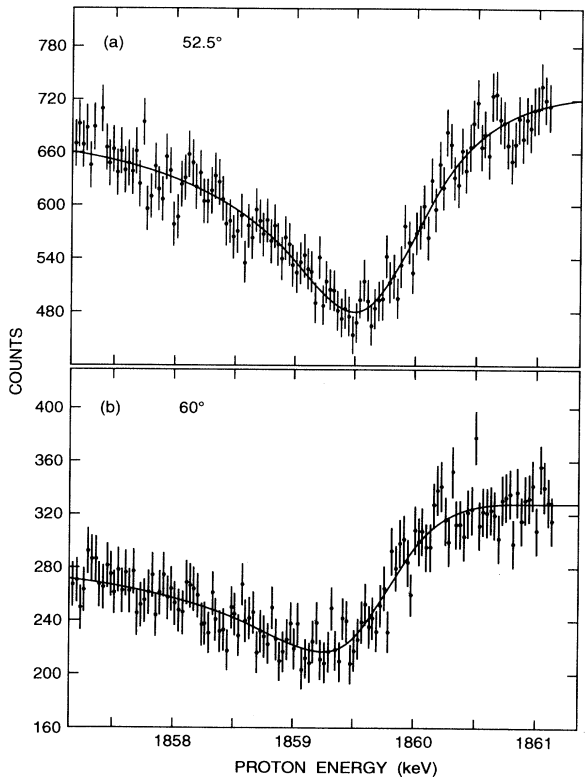

FIG. 2. The elastic nuclear resonance ^{40}Ar$(p,p)^{40}$Ar at 1859.7 keV as seen at both laboratory observation angles: (a) 52.5°, (b) 60°. The solid curves represent least-squares fits to the data of Eq. (5) with the fitting parameters A, B, C, E_0, and Γ.

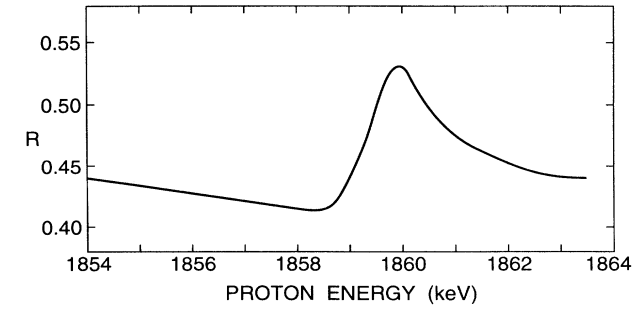

FIG. 3. The ratio $R(E,60°,52.5°)$ defined by Eq. (3) plotted as a function of the proton-impact energy. The value of R was derived from the fits to the resonances, as shown in Fig. 2.

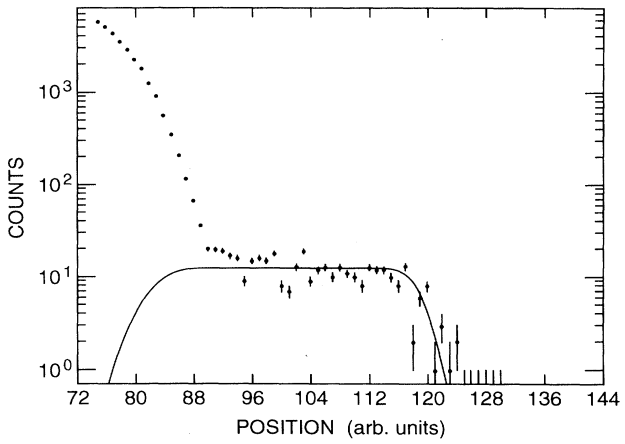

FIG. 4. Position spectrum for particles scattered at 60°. Protons to the left and neutral H^0 to the right are readily distinguished. The curve is a least-squares fit to the right part of the spectrum (see text for more details).

tinuous scan over the entire 4-kV range allowed monitoring of the position of the resonance. Due to remaining small variations in quadrupoles, steerers, and accelerator-voltage settings, the position of the resonance moves slightly over a period of several hours. Therefore the data were taken in a number of runs of around 2-h duration each. Individual runs, for which the position of the resonance has shifted less than 100 eV, were added to obtain better statistics. In this way, the uncertainties produced by the long-term drifts were kept at a minimum.

In Fig. 4 an example is shown of one of the position spectra. The large enhancement on the left-hand side is due to protons intercepted by the detector in spite of the deflection by the permanent magnet. The flat, low part on the right-hand side is produced by neutral H^0. The number of neutral particles $n^0(E,\theta)$ required in Eq. (4) was obtained by fitting the flat part by an analytical function, giving the shape of the position spectrum for the neutrals. This function was obtained from spectra accumulated without the permanent magnet. In this way, as seen in Fig. 4, the neutrals lying under the tail of the protons are taken into account. The data of Fig. 4 are the result of 12 h of measurement and correspond to a proton energy of 1859.55 keV.

III. RESULTS AND DISCUSSION

Figure 5 shows the measured electron-capture probability as a function of the proton-impact energy for the reaction $^{40}Ar(p,p)^{40}Ar$. Each group of five points with identical signature represents a set of data obtained as described in the preceding section. The vertical error bars account for statistical errors due to counting statistics alone, and the horizontal ones are the standard deviation of the position of the resonance obtained from the least-squares fits of Eq. (5) for the continuous energy scans of the resonance done periodically during the measurements. The partial overlap of protons and H^0 leads to an estimated systematic error of 20% or less. The probabilities at the extreme right and left ends of Fig. 5 give off-resonance atomic-electron-capture probabilities. When this value is compared to the interpolated value of the dip, an excursion of around 27% is obtained.

For a better understanding of the capture process itself, it is important to know the off-resonance electron-capture probability for a range of scattering angles and energies. Figure 6 shows such probabilities for 1.0-, 1.5-, and 2.0-MeV proton-impact energy and angles ranging from 6° to 60°. The data were taken earlier with different experimental arrangements but have not been published before. The open circle at (60°, 1.85 MeV) is the off-resonance value obtained in the present experiment (Fig. 5). The most remarkable trend seen in these experimental data is the strong decrease of the capture probability as the defection angle increases. This trend is seen also in the IA model [24]. A similar effect was noticed earlier for other targets [20]. The absolute values of the data in Figs. 5 and 6 do not seem to match smoothly. The apparent discrepancy of 10–20 % is most likely due to the different systematic errors of the techniques used.

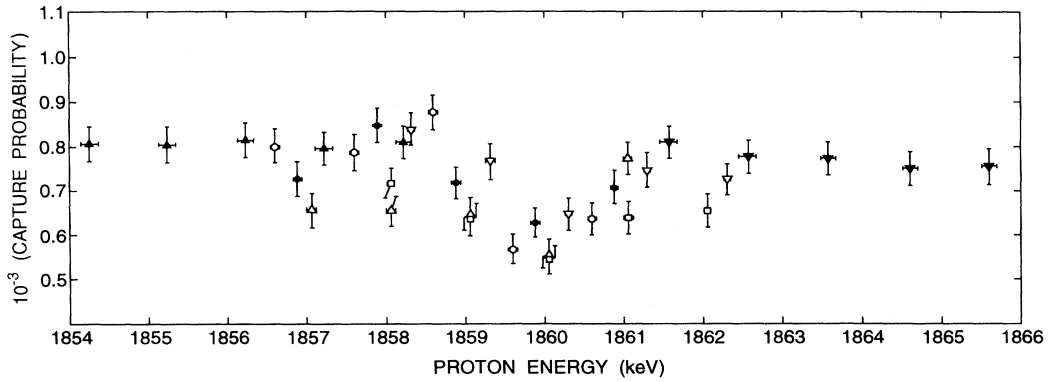

FIG. 5. Atomic-electron-capture probability as a function of the proton-impact energy near an elastic nuclear-scattering resonance, $^{40}Ar(p,p)^{40}Ar$. The different signatures identify seven different groups of five points, each obtained in seven different runs. Each run took up to 24 h of beam time, and the runs were taken over a period of several months.

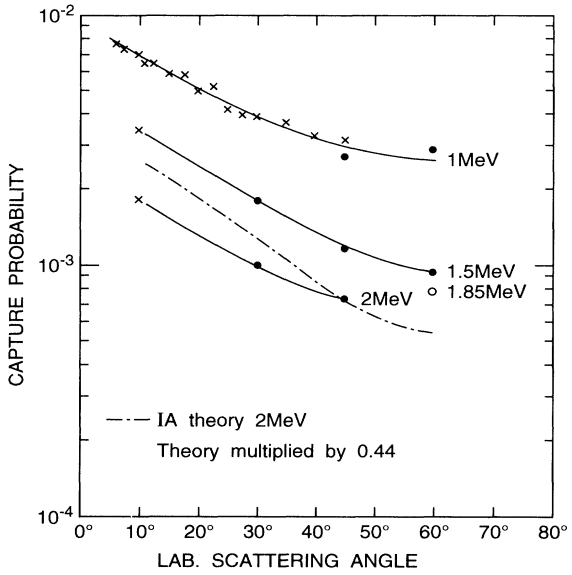

FIG. 6. Off-resonance atomic-electron-capture probability for 1.0-, 1.5-, and 2.0-MeV impact energies as a function of the scattering angle in $p+$Ar collisions. Off-resonance values from Fig. 5: ○. The other data were taken previously, using different experimental techniques, as discussed in Ref. [20]: ×, and Refs. [15] and [16]: ●. The dot-dashed curve is the result of the IA theoretical approach [7,24].

The influence of the nuclear resonance on the atomic process depends on the resonance strength, and this in turn depends on the nature of the resonance and on the deflection angle, e.g., for the same reaction, measurements at forward directions give weaker resonances than at backward scattering angles. Therefore, to compare the present results with previous ones for different reactions and different scattering angles, it is necessary in some way to normalize the excursion of the atomic-electron-capture probability at the resonance energy to the excursion of the proton-scattering cross section from the Rutherford cross section at the same energy. Table I shows a summary of previous data and a comparison with the present results. The excursions of the proton-scattering cross section and the capture probability are expressed as $(y_{max}-y_{min})/y_{off}$, where y_{max} and y_{min} are the maximum and minimum values of the probabilities/scattering cross sections in the energy region of the resonance and y_{off} is the off-resonance value.

Table I shows that for the reactions studied so far, an excursion of the capture probability across an elastic resonance is seen only in those cases for which ΔE and Γ are comparable. In addition, the normalized excursion clearly tends to increase as $\Delta E/\Gamma$ increases. A comparison between the ^{20}Ne and ^{22}Ne resonances seems to present an exception. However, it should be noted that in these cases, both the K and L shell contributes to the capture process [20–22] but not in equal proportion due to the different proton energies. Therefore a detailed comparison is difficult to make. The question cannot be settled by the theoretical results either, because the two available theories give different results, and, in addition, both disagree with the data [23] for the resonance on ^{22}Ne.

Careful inspection of Fig. 5 reveals systematic differences of the order of 10% between individual runs. These differences were eliminated by fitting of Eq. (5) to the five points of each of the five runs covering the resonance at 1859.7 keV. Only parameters A, B, and C were varied, while E and Γ were fixed at 1859.7 keV and 1288 eV, respectively. The probabilities measured in each run were then multiplied by the ratio C_{off}/C, where C_{off} is the off-resonance probability found in the two off-resonance runs below and above the resonance. The result is shown in Fig. 7 and compared with a theoretical prediction based on the IA approximation [7,24]. The theoretical curve includes incoherent contributions from $1s$ as well as from $2s$ and $2p_{0,1}$ electrons. The $2s$ and $2p_1$ electrons contribute about equally to the total probability ($2\times 38\%$), the $1s$ electrons are of secondary importance ($\sim 20\%$), and the contribution from the $2p_0$ electrons is

TABLE I. Parameters for nuclear reactions studied in conjunction with charge transfer in atomic collisions. The parameters θ_{lab}, E_0, and Γ are the observation angle, the resonance energy, and the width of the resonance, respectively. The quantity ΔE is the energy transfer associated with the charge transfer, and the parameter $\Delta E/\Gamma$ measures this quantity relative to the width of the resonance for electrons transferred from the K or L shell of the respective atoms. The excursions of the elastic-scattering cross sections (1) and the charge-transfer probabilities (2) are measured relative to the off-resonance values, as described in the text. The ratio (2)/(1) is a measure of the influence of the nuclear resonance on the charge transfer.

Reaction	Reference	θ_{lab} (deg)	E_0 (keV)	Γ (keV)	$\Delta E/\Gamma$		Excursion		
					K	L	Scatt. res. (1)	Capt. prob. (2)	Ratio (2)/(1)
^{12}C$(p,p)^{12}$C	[12,13]	150	462	35	0.015		1.7	0.05	0.03
^{14}N$(p,p,)^{14}$N	[12,13]	150	1058	6	0.16		1.2	0.4	0.33
^{20}Ne$(p,p)^{20}$Ne	[15]	30	1955	4	0.5	0.25	0.46	0.3	0.65
^{22}Ne$(p,p)^{22}$Ne	[13,14]	150	1510	2.45	0.7	0.35	2.1	0.7	0.34
^{40}Ar$(p,p)^{40}$Ar		60	1860	1.288		1	0.37	0.27	0.74

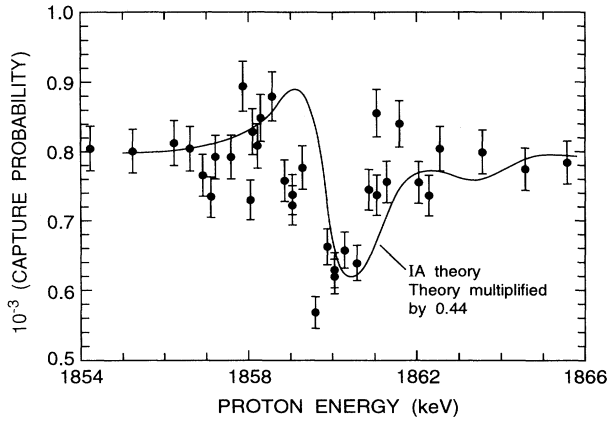

FIG. 7. Same data as in Fig. 5 corrected as described in the text. The solid curve is the result of the IA theoretical approach [7,24].

almost negligible ($\sim 4\%$). The different electronic shells show different resonance shapes and strengths. The shape of the curve shown in Fig. 7 is close to the shape of the $2p_1$ contribution alone. The magnitude of the resonance agrees reasonably well with the data, but there seems to be some discrepancy between the shapes, and the theory overestimates the data by about a factor of 2. It is therefore not clear how significant the agreement in the magnitude of the resonance is. Also the transverse-peaking approximation has been introduced in evaluating the IA theory. The effect on the results of this extra approximation is not known very well at present.

Table I shows that the scattering into backward angles gives rise to much more intense resonances than scattering in the forward direction. Therefore, from this point of view, scattering at backward angles seems favorable for the study of the interplay between atomic and nuclear processes. This is most likely true in the case of atomic inner-shell ionization where the reaction amplitude may be decomposed into an incoming ($t<0$) and an outgoing ($t>0$) amplitude which are related simply by $a_{\text{out}}=a_{\text{in}}^{*}$ [25], but for electron capture, such a simple relation does not exist. On the contrary, the time of excitation of the electron ($t=t'$) as well as the time of the nuclear scattering ($t=0$) is important, leading to three capture sequences (*enc*, *nec*, and *ecn*), as discussed in the Introduction, instead of the two for inner-shell ionization. Furthermore, the partial capture amplitudes depend differently on the deflection angle. The nature of the interplay between the nuclear scattering and the charge transfer is therefore sensitive to the scattering angle, thus it is desirable that future experiments be done over a range of deflection angles and not only at angles giving the largest resonance effect.

IV. CONCLUSIONS

A comparison between all the experimental data available to date on charge transfer across nuclear resonances supports the theoretical conclusion that the condition stated in Eq. (1) for a strong interplay between charge transfer and nuclear resonance is a necessary condition, and the condition also seems to be sufficient. However, a detailed understanding requires more experimental data of a systematic nature and with improved accuracy and resolution. The data should preferably address the angular dependence of the interplay, about which very little is known at present, and, if possible, separate the incoherent contributions from the various atomic shells. Based on the limited number of comparisons between theory and experiment [8], the generalization of the two-amplitude Blair-Anholt theory for pure ionization across a nuclear resonance to the case of charge transfer seems at present to be at least as successful as the more sophisticated SPB or IA approaches. Whether this could be due to the extra peaking approximations made in evaluating the SPB theory is not known at present.

ACKNOWLEDGMENTS

The authors would like to express their gratitude to D. H. Jakubassa-Amundsen for communicating unpublished theoretical results and for valuable comments on the manuscript prior to publication. We acknowledge the Danish Natural Science Research Council (SNF) for supporting A.D.G. and J.P.G.

*Also at CONICET, Buenos Aires, Argentina.
†Permanent address: J. R. Macdonald Laboratory, Kansas State University, Manhattan, KS 66506.

[1] For a review of inner-shell processes near nuclear reactions, see W. E. Meyerhof and J. F. Chemin, Adv. At. Mol. Phys. **20**, 173 (1985).
[2] For a general review on the interplay between atomic and nuclear processes, see U. Heinz, Rep. Prog. Phys. **50**, 145 (1987).
[3] L. Kocbach, *Brasov International School, Lecture Notes* (Brasov, Rumania, 1984).
[4] D. H. Jakubassa-Amundsen, Int. J. Mod. Phys. **A4**, 769 (1989).
[5] P. A. Amundsen and D. H. Jakubassa-Amundsen, Phys. Rev. Lett. **53**, 222 (1984).
[6] D. H. Jakubassa-Amundsen and P. A. Amundsen, J. Phys. B **18**, 757 (1985).
[7] D. H. Jakubassa-Amundsen, J. Phys. B **24**, 3019 (1991).
[8] O. Fojón and J. M. Maidagan, J. Phys. B **24**, 2529 (1991).
[9] Equation (5.1) of Ref. [6].
[10] Equation (29) of Ref. [8].
[11] E. Horsdal-Pedersen, P. Loftager, and J. L. Rasmussen, J. Phys. B **15**, 4423 (1982).
[12] J. N. Scheurer, O. K. Baker, and W. E. Meyerhof, J. Phys. B **18**, L85 (1985).
[13] O. K. Baker, C. Stoller, W. E. Meyerhof, and J. N. Scheurer, Nucl. Instrum. Methods Phys. Res. B **24/25**, 89 (1987).
[14] O. K. Baker, W. E. Meyerhof, D. W. Spooner, Ch. Stoller, and J. N. Scheurer, Phys. Rev. Lett. **60**, 913 (1988).

[15] E. Horsdal-Pedersen, B. Jensen, and K. O. Nielsen, Phys. Rev. Lett. **57**, 675 (1986).
[16] E. Horsdal-Pedersen, Nucl. Instrum. Methods Phys. Res. B **24/25**, 130 (1987).
[17] A. D. González, J. P. Giese, and E. Horsdal-Pedersen, Nucl. Instrum. Methods Phys. Res. B **71**, 224 (1992).
[18] The ΔE values are calculated using the binding energies given by E. Clementi and C. Roetti, At. Data Nucl. Data Tables **14**, 177 (1974).
[19] R. Bloch, T. Knellwolf, and R. E. Pixley, Nucl. Phys. A **123**, 129 (1969).
[20] E. Horsdal-Pedersen, P. Loftager, and J. L. Rasumssen, J. Phys. B **15**, 2461 (1982).
[21] D. H. Jakubassa-Amundsen, J. Phys. B **14**, 2647 (1981).
[22] E. Horsdal-Pedersen, F. Folkmann, and N. H. Pedersen, J. Phys. B **15**, 739 (1982).
[23] Figure 5 of Ref. [8] summarizes both the data and the various theoretical results.
[24] D. H. Jakubassa-Amundsen (private communication).
[25] See Ref. [1], Sec. V.